SPE 75533

X-ray Computed Tomography Observation of Methane Hydrate Dissociation

Liviu Tomutsa, SPE, Barry Freifeld, Timothy J. Kneafsey, Lawrence Berkeley National Laboratory, Laura A. Stern, United States Geological Survey

This paper was prepared for presentation at the SPE Gas Technology Symposium held in Calgary, Alberta, Canada, 30 April–2 May 2002.

Abstract

Deposits of naturally occurring methane hydrate have been identified in permafrost and deep oceanic environments with global reserves estimated to be twice the total amount of energy stored in fossil fuels. The fundamental behavior of methane hydrate in natural formations, while poorly understood, is of critical importance if the economic recovery of methane from hydrates is to be accomplished. In this study, computed X-ray tomography (CT) scanning is used to image an advancing dissociation front in a heterogeneous gas hydrate/sand sample at 0.1 MPa. The cylindrical methane hydrate and sand aggregate, 2.54 cm in diameter and 6.3 cm long, was contained in a PVC sample holder that was insulated on all but one end. At the uninsulated end, the dissociated gas was captured and the volume of gas monitored. The sample was initially imaged axially using X-ray CT scanning within the methane hydrate stability zone by keeping the sample temperature at 77°K. Subsequently, as the sample warmed through the methane hydrate dissociation point at 194°K and room pressure, gas was produced and the temperature at the bottom of the sample plug was monitored while CT images were acquired. The experiment showed that CT imaging can resolve the reduction in density (as seen by a reduction in beam attenuation) of the hydrate/sand aggregate due to the dissociation of methane hydrate. In addition, a comparison of CT images with gas flow and temperature measurements reveals that the CT scanner is able to resolve accurately and spatially the advancing dissociation front. Future experiments designed to better understand the thermodynamics of hydrate dissociation are planned to take advantage of the temporal and spatial resolution that the CT scanner provides.

Introduction

In the oil and gas industry, gas hydrate research has traditionally focused on designing improved methods to prevent its formation in conduits where it impedes fluid transport in subsea or permafrost operations (1,2,3). More recently, the interest in hydrates has been directed towards understanding of the vast potential of gas hydrates as a natural gas resource (4). Field, laboratory, and theoretical work have begun to focus on the many aspects of gas hydrates including reserve evaluation, hydrate recovery, gas production, hydrate formation, hydrate properties, dissociation, depressurization modeling, and thermal gas production from hydrates (5). To help refine current models of gas production from natural gas hydrate accumulations (6), a better understanding of the physical processes that occur during methane hydrate dissociation is critically important. Many physical and hydrologic properties of hydrate/sediment aggregates require evaluation to gain a further understanding of the potential for gas recovery from hydrates. These properties include relative permeability, thermal conductivity, heat capacity, and compaction. While various aspects of gas hydrate formation and dissociation have been investigated on both natural (7) and synthetic (8,9) gas hydrate test materials, synthetic hydrates offer the advantage of better sample control and uniformity than natural materials. Furthermore, representative natural hydrate samples have proved to be very difficult to collect.

Imaging methods, such as X-ray Computed Tomography (CT), have been used to characterize naturally occurring hydrates (10) or to directly observe their dissociation while reducing the ambient pressure below the stability pressure (11). In this study, we describe CT scanning experiments on an aggregated sample of methane hydrate with quartz sand, and show how this technique can be used successfully to image an advancing dissociation front due to heat influx applied to one end of the sample, at a constant pressure of 0.1 MPa.

Methods

Sample fabrication and preparation

Test material of polycrystalline methane hydrate was synthesized by combining cold, pressurized CH_4 gas (250 K, 27 MPa) with granular H_2O ice "seeds" (typically 26 to 32 g, at 180-250 μm grain size) in stainless steel reaction vessels

[6,7]. Heating the ice + gas reactants above the H_2O melting point promotes *in situ* conversion of ice grains to hydrate grains by the general reaction CH_4 (g) + $5.9H_2O$ (s $\rightarrow$ l) $\rightarrow$ $CH_4 \cdot 5.9H_2O$ (8,9). Complete reaction was attained by continued warming to 290 K and ~30 MPa for approximately 12 to 15 hours. During hydrate synthesis, sample temperature (T) was monitored by axially positioned thermocouples in side-by-side companion samples, and methane gas pressure (P_{CH4}) was monitored by a Heise bourdon gauge and pressure transducers. Complete reaction was determined from the *P-T* synthesis record, as hydrate formation consumes a known mass of the vapor phase and thus causes a predictable pressure offset in the *P-T* record. Samples were then cooled back to 250 K, and the lack of discontinuities in their thermal profiles upon crossing the ice point provided further substantiation that no measurable unreacted H_2O ice remained. The resulting hydrate product is highly reproducible in composition as well as in grain and pore characteristics; test specimens are nearly pure (> 99 vol. %), porous (~ 29%) cohesive cylinders of 2.54 cm in diameter by 9 to 12 cm in length, depending on the initial amount and packing of the seed ice (Figure 1). The hydrate has controlled grain size, random crystallographic orientation, and no detectable secondary phases.

The methane hydrate/quartz sand samples used in this experiment were produced by mixing measured and pre-specified amounts of granular "seed" ice with quartz sand (100-150 μm grain size, Oklahoma #1), then packing the ice + sediment mixtures into the reaction vessels prior to admission of CH_4 gas (8). Using the same static growth method described above, no detectable migration of either the H_2O or sediment was observed during subsequent heating and conversion of the ice grains to hydrate grains. For the hydrate + quartz experiments described in the current study, all test material came from one initial sample, shown at right in Figure 1. For this sample, ice + sand grains were pre-mixed and packed as four discrete layers to yield final compositions of (from top to bottom): 75 vol. % hydrate + 25 vol. % sand; 60 vol. % hydrate + 40 vol. % sand; 40/60; 25/75. The top and bottom segments were removed and we only consider the solid material (methane hydrate and sand) in our classification of the samples as 40% sand/60% hydrate etc. All layers were relatively porous (~49%).

Test procedures

The sample used in our experiment was a 2.54 cm diameter x 6.3 cm long composite with about half of the sample composed of 60%/40% sand/hydrate (by volume), and the other half 40%/60% sand/hydrate (by volume). Note that we do not include porosity in these descriptions.

A gas-tight PVC sample holder with plastic fittings was constructed to contain the sample (Figure 2). Materials were selected to minimize X-ray attenuation. A sheathed type-J thermocouple was inserted through the sample holder bottom such that the sample would rest in contact with the thermocouple tip. The sample holder top was connected to the gas collection system. The sample holder was set into an insulating Styrofoam container and stabilized with Styrofoam wedges.

We carried out the experiment by first CT scanning the sample holder while empty. Before inserting the sample, the sample holder was cooled by pouring liquid nitrogen into the surrounding Styrofoam container. The sample was then placed in the sample holder, and the end cap screwed into place. The tube to the gas collection system was connected, the time clock started, and measurements begun. Initial scans were made while maintaining the temperature at the liquid nitrogen boiling point. We continued to scan the sample while allowing the nitrogen to boil off. When sufficient nitrogen had evaporated, the temperature at the sample bottom began to increase. We continued to scan the sample as the temperature increased and hydrate dissociation commenced. The gas volume evolved from the sample was measured by collection in a calibrated Mariotte bottle. The displaced water from the Mariotte bottle was captured in a reservoir which was continuously weighed. The composition of the gas was measured following dissociation.

A Siemens Somaton HiQ medical CT scanner was used to obtain the X-ray CT data. Axial cross sections 1mm thick were obtained by scanning the vertically oriented sample with an X-ray energy of 133keV at a current of 120 mA. The voxel size in each image was 1mm x 0.2mm x 0.2mm. Repeated scans of a near-center plane were performed to monitor changes over time. The duration of each scan was 4 seconds and the time interval between the scans varied from a few minutes during pre- and post-dissociation phases to a few tens of seconds during the hydrate dissociation phase. Data was transferred from the CT scanner through an ethernet link to personal computers for processing. Data obtained were reviewed and processed to enhance visualization of the processes that occurred. Typically the image processing included subtraction of an initial data set to look at changes between the two scans. The software used for data manipulation and visualization consisted of custom and commercial packages including Spyglass Transform™, Tecplot™, and Excel™.

Results

X-ray Computed Tomography

Initially, the sample was maintained within the stability region of the methane hydrate at the normal nitrogen boiling point (77 K) to establish a baseline CT attenuation data set. As the temperature of the sample was allowed to increase above the boiling point of liquid nitrogen, but still presumably within the stability region of the methane hydrate, we noted reductions in beam attenuation that coincided with the evolution of gas into the Mariotte bottle. We interpreted this to indicate the presence of nitrogen within the sample, which was subsequently confirmed with the chemical analysis of the

evolved gas. We determined that, the nitrogen boiled off resulting in a noticeable change in subsequent scans. The liquid nitrogen within the sample boiled off after 45 minutes (Image 64 in Figure 3), coinciding with the time when the temperature of the bottom of the sample rose above the nitrogen boiling point.

The changes in the sample X-ray attenuation between consecutive scans were difficult to discern because of the small attenuation differences between the gas hydrate/sand mixture and the resulting ice/sand mixture that formed during dissociation. However, after processing of the CT data by differencing the images with the baseline data, the hydrate dissociation could be resolved and the advancing dissociation front could be clearly distinguished. Figure 3 presents the results of an evaluation of the difference data sets corresponding to movement of the dissociation front through the sample for a few selected CT scans.

To further study the time dependence of the advancing front, so that the front, temperature, and gas production could be presented together, the average X-ray attenuation of the central 60 percent of the sample was plotted over the duration of the experiment using all the CT scans (Figure 4). The center 60% was selected so as to avoid effects of radial warming that might occur at the edge of the sample. In Figure 4, the average attenuation difference at each elevation is plotted over time. Thus a change in attenuation caused by the advancing dissociation front would be seen as a curve between regions of different attenuation (shades of gray). The linearity of the movement of the dissociation front in this sample is striking. Using the CT data, we also investigated whether the front also moved radially through the sample. We used the averaged data over 1 mm in height for two locations; one located centrally in the top (~1 cm below the sample top), and the other located about 1.5 cm below the interface between the 60%/40% sand hydrate and 40%/60% sand/hydrate portions of the sample. The results, shown in Figure 5, indicate that the dissociation front was relatively sharp and horizontal, thus there was no radial movement of the front.

In the X-ray difference scans, towards the top of the sample (see Figures 3 and 4), a band of increasing X-ray attenuation gets thicker as the temperature increases and dissociation occurs. We attribute this change to expansion of the sample as temperature increased, due in part to the rapid release of gas accompanying dissociation. The reason for the high attenuation difference values is that the expanded sample attenuates X-rays much more strongly than the gas that previously occupied that location. At the interface between the 60% sand (top) and 40% sand (bottom) a decrease in attenuation is observed which is consistent with expansion.

Temperature History

In addition to X-ray attenuation changes, Figure 4 shows the temperature at the bottom of the sample over the duration of the experiment. Initially, the sample contained liquid nitrogen at the bottom, and remained at the normal boiling point. During this time period, liquid nitrogen was also applied in the Styrofoam container to cool the sample holder and sample. When the liquid nitrogen in the sample boiled off (after about 90 minutes), the temperature increased fairly uniformly at a rate of about 1.2^{o}C/min until about 125 minutes. After 125 minutes, the rate of temperature increase declined to about 0.9^{o}C/min until the sample bottom reached the dissociation point at about 135 minutes. Because the dissociation of methane hydrate is endothermic, this change of rate could be due to either the dissociation phase change, or to the increased amount of hydrate in the lower part of the sample. Another slight decrease in the rate of temperature increase is observed at 171 minutes at a temperature of 237 K, although this rate change is smaller than the one at 135 minutes.

Gas Production

The gas production curve overlies the CT data in Figure 4. It is clear that the methane hydrate in the sample began dissociation and gas was collected 90 minutes after the start of the experiment. The temperature of the sample bottom at 90 minutes is well below the dissociation temperature (194 K) indicating that the dissociation was occurring elsewhere in the sample. Gas collection continued until 143 minutes. At that time, the temperature at the bottom of the sample where the final hydrate dissociated was just over 200 K. Following the end of this primary dissociation event, the differences noticed in the enhanced CT scans were minimal.

For the first 90 minutes of the experiment, gas was generated at about 6.4 ml/min. We attributed this primarily to nitrogen gas resulting from boiling liquid nitrogen in the sample. After 90 minutes, a marked increase in gas production was observed (to about 23.5 ml/min). After about 124 minutes, the rate again increased (to about 31.8 ml/min) even with the lower rate of temperature increase. The total gas produced prior to 90 minutes was about 360 ml. By 124 minutes an additional volume of 782 ml was produced, and after 124 minutes 582 ml of gas was produced.

The gas composition in the bottle was measured using a LandTec GEM 2000 landfill gas analyzer. By subtracting off the initial gas in the Mariotte bottle, we determined that 1120 ml of methane and 630 ml of nitrogen were produced (at room temperature and pressure). This implies that about 0.75g (~1 ml liquid if in that form) of nitrogen was initially present. The volume of nitrogen ultimately produced significantly exceeds the amount of nitrogen produced when the temperature first exceeded the nitrogen boiling point (~260 ml), indicating that nitrogen was present in a significant quantity but apparently not in free liquid or gas form. It is not clear what form the nitrogen in the sample was in or when during the experiment it entered the collection bottle. We note, however, that the particular sample we used was stored in liquid nitrogen for almost two years prior to its use. While

nitrogen is known to sorb to surfaces and also to form hydrates, we note that nitrogen hydrate typically forms only under elevated N_2 pressures, forming a type II rather than type I clathrate hydrate.

Discussion

The aim of this experiment was to determine the usefulness of X-ray CT imaging in differentiating between methane hydrate in a porous media and the same porous media with the hydrate dissociated and transformed into water ice. We successfully demonstrated that X-ray CT imaging is extremely useful in observing the dissociation process even in an aggregated sand-hydrate sample. The challenge lies in the large attenuating potential of the mineral grains (a function of density) which masks the relatively modest decrease in density that accompanies the change from gas hydrate to water ice. The reduction in density that accompanies hydrate dissociation for the sample investigated in this study is 4.7% for the 60% sand/40% hydrate portion of the sample and 8.7% for the 40%sand/60% hydrate portion of the sample. To calculate the density reduction it is assumed that the bulk structure is maintained by the sand/ice matrix upon complete dissociation of the hydrate without any displacement of the mineral grains. Both the small changes in density, and mechanical deformation must be considered when CT scanning representative natural gas hydrate samples. Further experience with synthetic samples will provide the background knowledge to scan natural samples retrieved under natural conditions and maintained without allowing hydrate dissociation to determine their physical structure.

Conclusions

This study presents spatial and temporal visualization of a methane hydrate dissociation front advancing in a synthetic hydrate/sand aggregate using computed X-ray tomographic scanning, and confirms previously work on natural samples (11). CT scanning can provide a useful tool for observing and measuring hydrate dissociation. The changes in the X-ray beam attenuation are shown to be sufficiently large to overcome the challenge posed by the high-density mineral grains. The volume and composition of the evolved gas provides further evidence that the X-ray tomographic images are accurately tracking the dissociation front. This study opens up the possibility of experiments combining three-dimensional X-ray CT visualization with measurement of thermodynamic parameters to further the understanding of the complex processes that underlies methane hydrate dissociation in porous media. Additionally, the development of broader experience with gas hydrates using CT scanning will enable nondestructive examination of natural samples.

Acknowledgments

The authors would like to thank the Department of Energy for supporting this work and Larry Myer, George Moridis and Steve Kirby for their input. We also thank John Apps for his careful review and thoughtful comments.

References

1. Sloan, E.D., Jr: *Clathrate Hydrates of Natural Gases*, second Ed., Marcel Dekker, Inc. New York, USA (1998)

2. Paez, J.E., R. Blok, H. Vaziri, and M.R. Islam, Problems in Hydrates: Mechanisms and Elimination Methods. SPE 67322, Presented at the SPE Production Operations Symposium held in Oklahoma City, Oklahoma, 26-28 March 2001.

3. Sinquin, A, X Bredzinsky, and V. Beunat, Kinetic of Hydrates Formation: Influence of Crude Oils. SPE 71543, Presented at the 2001 Annual Technical Conference and Exhibition held in New Orleans, Louisiana, 30 September - 3 October 2001

4. Allison, E., Department of Energy Methane Hydrate Research and Development Program, in *Gas Hydrates, Challenges for the Future,* G.D. Holder and P. R. Bishnoi, ed., Annals of the New York Academy of Sciences, v. 912, 2000, pp. 437-440.

5. Ripmeester, J.A. Hydrate Research- From Correlations to Knowledge-Based Discipline, The importance of Structure, *Gas Hydrates, Challenges for the Future*, G.D. Holder and P. R. Bishnoi, ed., Annals of the New York Academy of Sciences, v. 912, 2000, pp. 1 – 16.

6. Swinkels, W.J.A.M, and R.J.J. Drenth, Thermal Reservoir Simulation Model of Production From Naturally Occurring Gas Hydrate Accumulations. SPE68213 SPE Reservoir Eval&Eng. **3** (6) December 2000, pp. 559-566.

7. Ohara, T. , S. R. Dallimore, and E. Fercho JAPEX/JNOC/GSC MALLIK 2L-38 Gas Hydrate Research Well, Mackenzie Delta, N.W.T. : Overview of Field Operations, SPE 59795 Presented at the 2000 SPE/CERI Gas Technology Symposium held in Calgary, Alberta Canada, 3–5 April 2000.

8. Stern, L. A., Kirby, S. H., Durham, W. B., Circone, S., and Waite, W. F., 2000, Synthesis of pure methane hydrate suitable for measurement of physical properties and decomposition behavior, Chapter 25, *Natural Gas Hydrate: In Oceanic and Permafrost Environments*, M.D. Max, ed., Kluwer publ., Dordrecht, p. 323-349.

9. Stern, L. A., Kirby, S. H., and Durham, W. B., 1996, Peculiarities of methane clathrate hydrate formation and solid-state deformation, including possible superheating of water ice, *Science*, vol. *273* (5283), 1843-1848.

10. Uchida, T. S, Dallimore, J. Mikami, Occurrences of Natural Gas Hydrates beneath the permafrost Zone in Mackenzie Delta, Visual and X-ray CT Imagery, *Gas Hydrates, Challenges for the Future*, G.D. Holder and P.R. Bishnoi, eds., Annals of the New York Academy of Sciences, Vol. 912, 2000, pp. 1021-1033.

11. Mikami, J., Y. Masuda, T. Uchida, T. Satoh, and H. Takeda, Dissociation of Natural Gas Hydrates Observed by X-ray CT Scanner, *Gas Hydrates, Challenges for the Futur*e, G.D. Holder and P.R. Bishnoi, eds., Annals of the New York Academy of Sciences, Vol. 912, 2000, pp. 1011-1020.

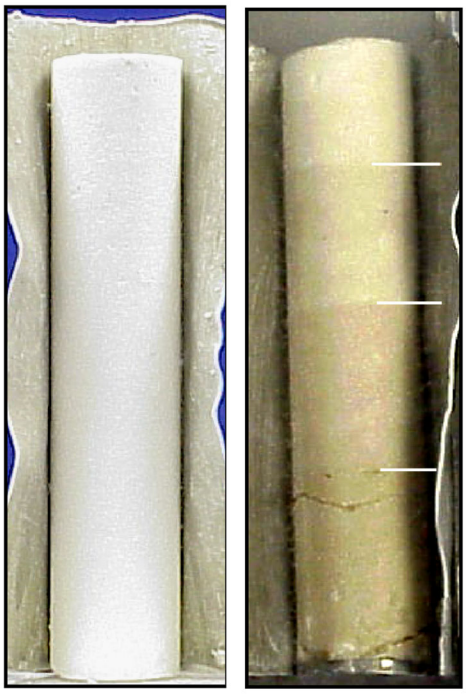

Figure 1. Synthetic pure methane hydrate (left) and quartz/ methane hydrate aggregate (right) samples. The vertical quadrants (delineated by white lines) have the following sand/hydrate proportions. Top section: 25 vol. % sand + 75 vol. % methane hydrate, mixed homogeneously as described in text. Second (upper central) section: 40 / 60. Third (lower central) section: 60/40. Base section: 75/25.

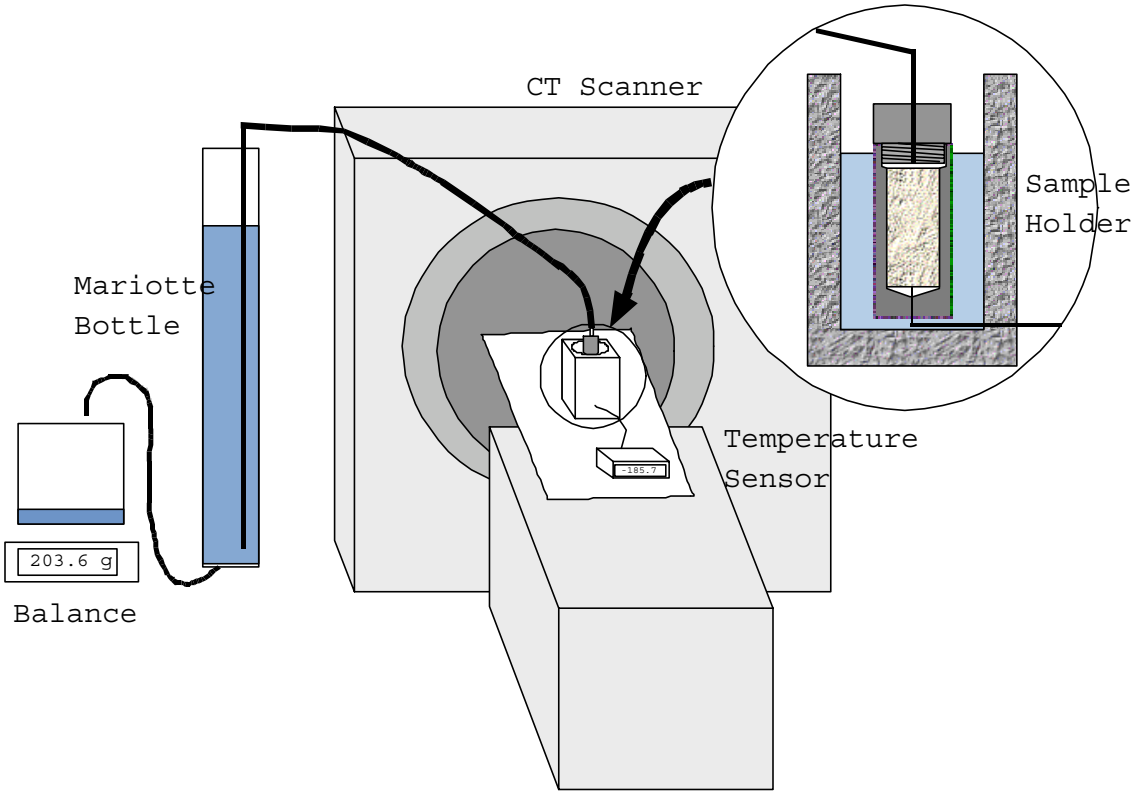

Figure 2. Schematic of the experimental setup, with a detail of the PVC coreholder surrounded by styrofoam insulation.

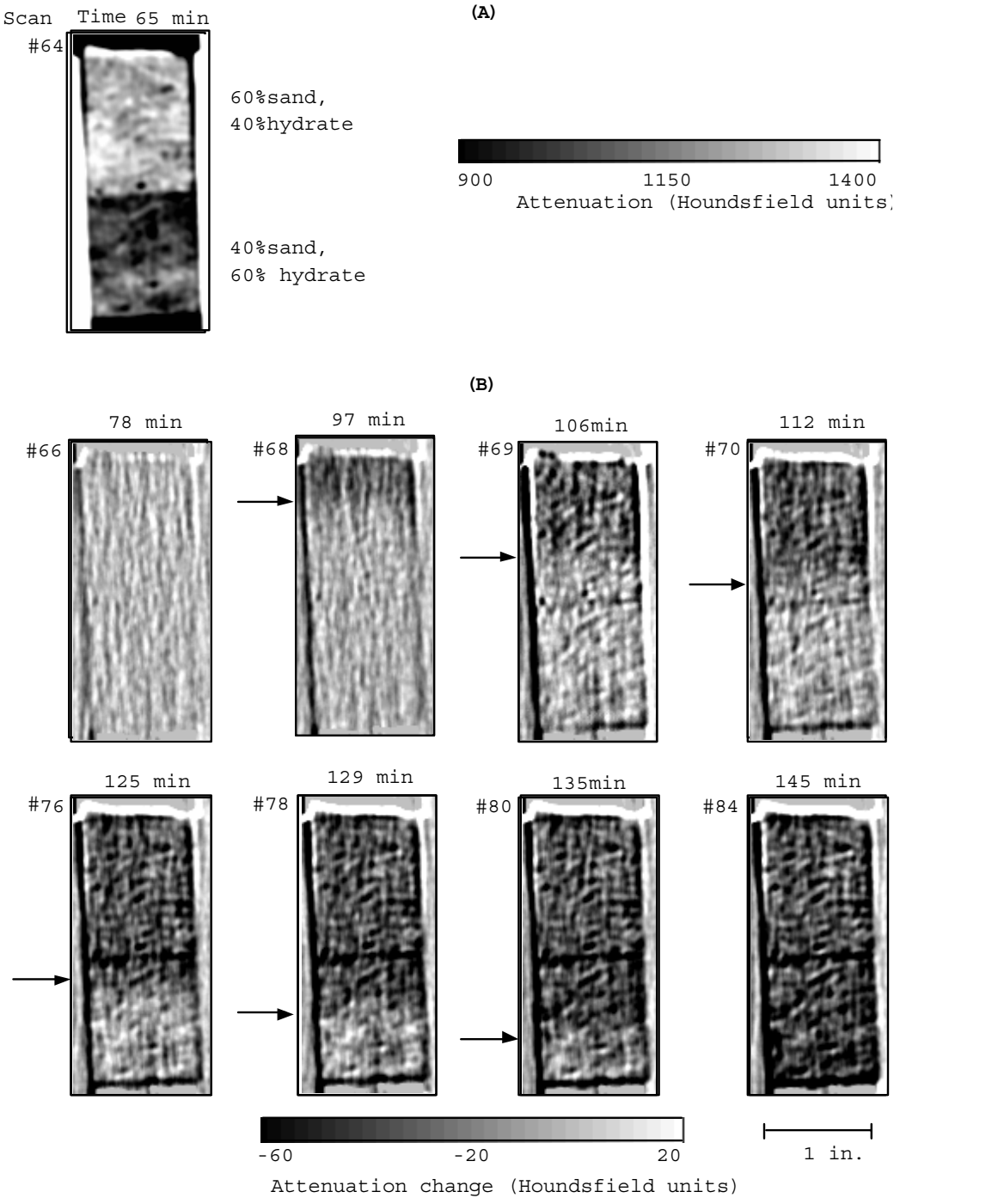

Figure 3. (A) X-ray CT image of the methane hydrate/quartz sample. (B) X-ray CT images showing attenuation changes as the dissociation front progresses downward in the methane hydrate sample. Images are all differences relative to scan #64.

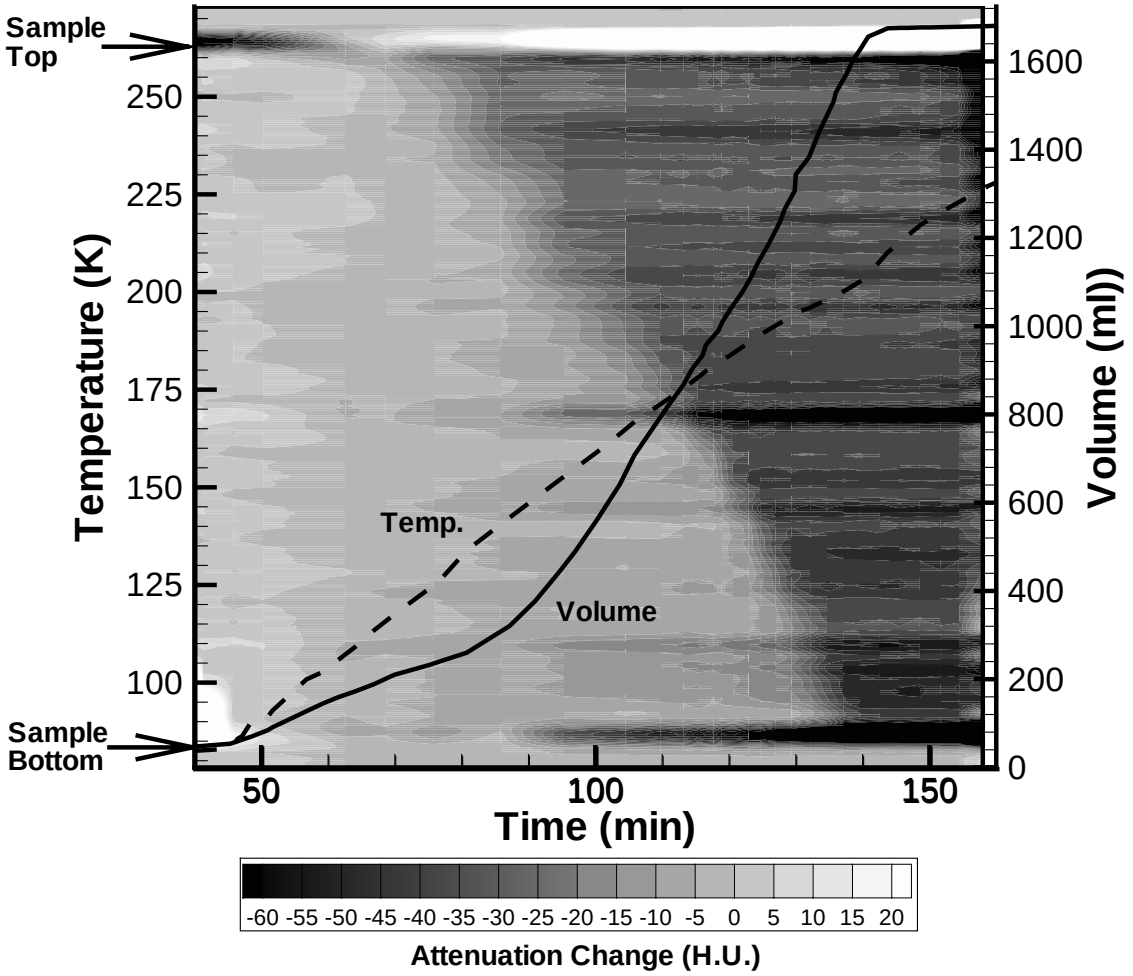

Figure 4. Composite image of an averaged vertical slice from each of the X-ray CT images of the methane hydrate sample, showing the dissociation front progressing downward. Horizontal pixels from the middle 15mm of the sample are averaged across each row to provide one value at each vertical location. Superimposed over the image is the total volume of gas evolved and the temperature at the bottom of the sample.

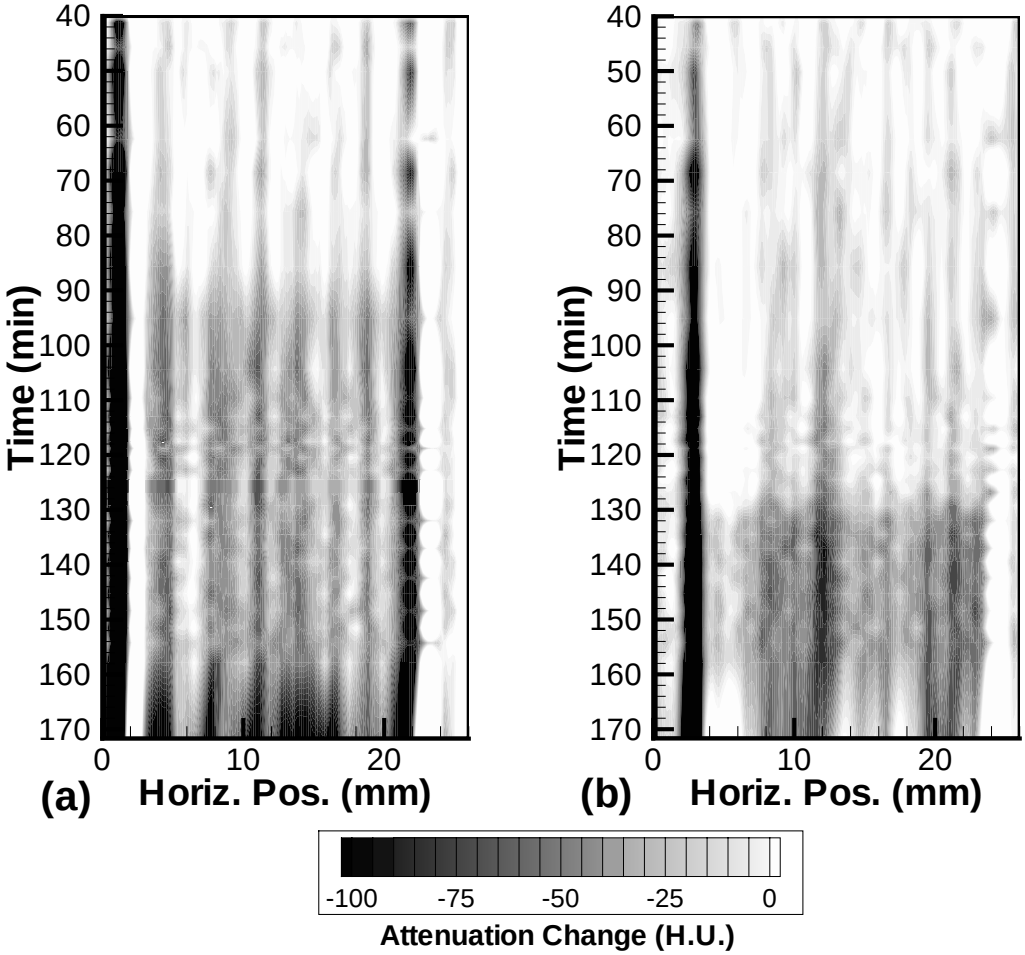

Figure 5. Composite images of averaged horizontal slices from X-ray CT images as the dissociation front progresses downward. Vertical pixels within a 1mm range are averaged to provide one value at each horizontal location. (a) horizontal slice ~1 cm below sample top (b) horizontal slice ~1.7 cm above sample bottom.